Tire X-ray Image Impurity Detection Based on Multiple Kernel Learning

Shuai Zhao[1,2], Zhineng Chen[2(✉)], Baokui Li[1], and Bin Zhang[3]

[1] School of Automation, Beijing Institute of Technology, Bejing 100081, China
zshuaibit@163.com, libaokui@bit.edu.cn
[2] Institute of Automation, Chinese Academy of Sciences, Bejing 100190, China
zhineng.chen@ia.ac.cn
[3] MESNAC Co., Ltd., Shandong 266042, China
zhangb1@mesnac.com

Abstract. Impurity detection on tire X-ray image is an indispensable phase in tire quality control and the widely adopted manual inspection could not attain satisfactory performance. In this work we propose an idMKL method to automatically detect impurities by leveraging multiple kernel learning (MKL). idMKL first applies image processing techniques to separate different regions of a tire image and suppress their normal texture characteristics. As a result, candidate blobs containing both true impurities and false alarms are obtained. We extract different features from the blobs and evaluate their effectiveness in impurity detection. MKL is then employed to adaptively combine the features to maximize the detection performance. Experiments on thousands of images show that idMKL can well separate the blobs and achieves promising results in tire impurity detection. Moreover, idMKL has been adopted as a mean complementary to the manual inspection by tire factories and shown to be effective.

Keywords: Tire X-ray image · Multiple kernel learning
Defect detection

1 Introduction

Tire is a basic equipment in vehicles. However, it is not rare that improper handles and unclean materials are involved in the tire manufacturing. As a result, tires may be contaminated by various defects, such as metallic and non metallic impurities (e.g., steel threads, screws, and plastic fragments), bubbles, etc. Statistics indicates that 40% of traffic accidents are relevant to tire quality [1]. Inspection based on the tire X-ray image is an important means for tire quality control, especially for defects inside rubbers. Currently, the inspection is performed manually in most tire factories. Nevertheless, a number of practices show that the human inspection, not only with high labor costs, still let many defects undetected because of not being easy to be observed, visual fatigue [2], etc. Automatic defect detection systems are highly demanded.

B. Zeng et al. (Eds.): PCM 2017, LNCS 10735, pp. 346–355, 2018.
https://doi.org/10.1007/978-3-319-77380-3_33

This work discusses detecting impurities, one major kind of defects on the tire. Impurity detection is a difficult task whose challenges mainly come from three aspects. First, a tire X-ray image is often with resolution of no less than 2200*10000 while many impurities occupy less than 100 pixels and with various shapes and intensities. Even skillful workers could not discover them well. Second, due to the complicated manufacturing process, the image exhibits many irregular and cluttered texture similar to impurities such that false alarms are easily reported. Third, there are hundreds of tire models. It is not easy to develop a generic algorithm that is capable of suppressing normal texture characteristics across the models.

In the literature, there are some research efforts dedicated to this task. Zhang et al. [3] propose an improved Canny edge detection scheme to detect impurities in tire X-ray image based on curvelet and the multiscale geometric transform. While later in [4], they proposed a method for detecting tire defects based on wavelet multiscale analysis. In [5], Xiang et al. present a dictionary based detection method by analyzing the distribution of representative coefficients. However, its performance heavily relies on parameters. Tajeripour et al. [6] and Kumar et al. [7] also propose detection methods which employ local binary pattern (LBP) to extract texture features. Despite progresses made, these efforts are somehow heuristic, especially at the level of handling candidate impurity blobs, i.e., determining which suspected blobs are impurities and which ones are false alarms. Moreover, They are only evaluated on dozens of to a few hundred tire images while no message shows these methods have been applied to the industrial, e.g., tire factories. We argue that the complex blob patterns (See Fig. 3) are difficult to describe by heuristics. It is advantageous to use machine learning techniques to distinguish them. However, they are totally ignored except for [8]. In this work, Xue et al. propose a topographic independent component analysis based method to extract discriminative features based on tire X-ray image, and then implement the defect detection by using support vector machine (SVM).

In this work we propose a novel idMKL method to detect impurities based on the tire X-ray image by leveraging multiple kernel learning (MKL) [9]. Specifically, given a tire image (Fig. 2(a) shows a fraction of an image), image processing techniques are applied first to segment the image to different functional regions from left to right. Since the regions are with quite different appearance, different strategies are applied to them separately to remove their normal texture for the sake of highlighting possible impurities, as shown in Fig. 2. As a result, candidate blobs containing both true impurities and false alarms are obtained. These blobs differ in location, size, sharp, intensity, etc. It is difficult to describe them by simple heuristics or features. To this end for each blob, we propose to extract multiple features from different image domains to acquire a complete but redundant description. Then, MKL is employed to distinguish these features and combine them in a weighted manner, where large weights are adaptively allocated to discriminative features while the weights for useless features are negligible. Experiments on thousands of images obtained from tire factories show that idMKL well separate the candidate blobs and achieves promising

results in detecting impurities from the whole tire X-ray image. Moreover, due to its superiority, idMKL has been equipped by tire factories to double inspect tire images passed the human inspection. It is shown that this novel tire quality control pipeline has played a more prominent role than human in tire inspection.

Contribution of this work is threefold: first, we propose to use MKL to model complex impurity patterns, where multiple useful features are appropriately combined and a powerful description is generated accordingly. To our knowledge, it is the first attempt that using MKL to detect tire impurities. Second, image processing and machine learning are appropriately integrated in the proposed idMKL. It forces machine learning to focus on distinguishing those small and hard-to-described blobs rather than the whole image thus leverages its merit. Third, comprehensive and rigorous evaluations are carried out on thousands of images, from which effectiveness of the proposed idMKL is verified by both large-scale data and the industrial.

2 The idMKL Method

2.1 Candidate Impurity Extraction

A tire is primarily composed of five functional regions including two tire beads, two sidewalls and a tread from left to right and from right to left [1]. Since different materials and processes are applied, these regions exhibit quite differently in the X-ray image, as shown in Fig. 2(a). Impurities may be contained in every part of the tire with diverse appearance. Typical examples are given by Fig. 1(a)–(f), where metallic, non metallic and overlap impurities on the three kinds of regions are depicted. By zooming in the image, it is also seen that some normal texture looks similar to impurities. Even human can not distinguish them well regardless of their spatial layouts, surrounding texture, etc.

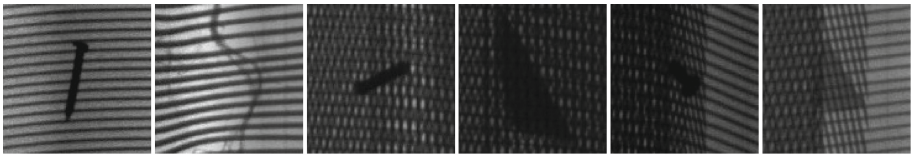

(a) (c) (c) (d) (e) (f)

Fig. 1. Typical X-ray image impurities (a)–(f)

Since textual characteristics are similar for the same kind of region but different for different regions, we propose a two-step pipeline to identify the possible impurities. First, the functional regions are segmented. Then, different textual removal strategies are separately applied to these regions, with the same purpose of highlighting possible impurities. In region segmentation, note that both bead and tread regions exhibit certain mash-like structures while the main pattern

in sidewall is horizontal steel cords. Morphological filtering method is applied at first to remove the steel cords as much as possible and histogram equalization column-by-column is also adopted meanwhile to highlight impurity areas as shown in Fig. 2(b). Then, local pixel scanning is carried out column-by-column at multiple scales, to find the appropriate local high pixel areas, as shown in Fig. 2(c) (the areas are marked by white). Since mash-like structures always correspond to many such small areas, and moreover, both bead and tread regions are darker than the sidewall, the region boundaries can be derived by jointly analyzing the distribution of small areas and column-projected pixel values. With regions segmented by the boundaries, classic image processing techniques including several kinds of filtering, connectivity analysis, binarization, etc., are appropriately assembled for every functional region to remove the normal texture and highlight possible impurity blobs, as shown in Fig. 2(d). Note that we only give a quite brief description of this part, as it is not the major contribution of this work.

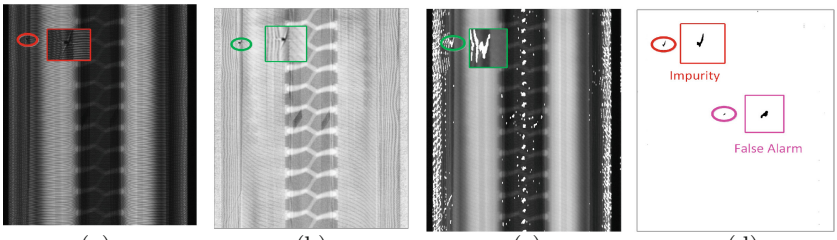

Fig. 2. Candidate impurity extraction pipeline. (a) Source image, (b) column-equalized image, (c) image with marked areas, (d) binary image with suspected impurities.

Since the extraction above is rather challenging, it is not surprise the generated blobs are composed of impurities, normal texture and small flaws that not affect the tire quality. It is difficult to distinguish them by simple features or heuristics, as no significant pattern can be observed from different kinds of blobs. The fact motivates us to employ machine learning techniques described below to address the problem.

2.2 Candidate Impurity Representation

By leveraging machine learning, a straightforward idea is to extract features from the blobs and then using SVM classification to distinguish impurities and false alarms including normal texture and small flaws. Typically, SVM use a kernel function to map the feature vector from low dimensional to high dimensional space, from which the classification boundary can be determined easier [10].

Choosing what features to represent the blobs is a critical issue. Intuitively, the blobs differ in size, sharp, intensity, etc. Typical color, geometric and texture

features are all useful in representing them. However, it is insufficient to describe them by using any of the features individually, as other kinds of features are also helpful apparently but missed. Moreover, we observe that there are many normal texture also looked similar to some impurities from the source tire image. It would be beneficial to extract features from other domains.

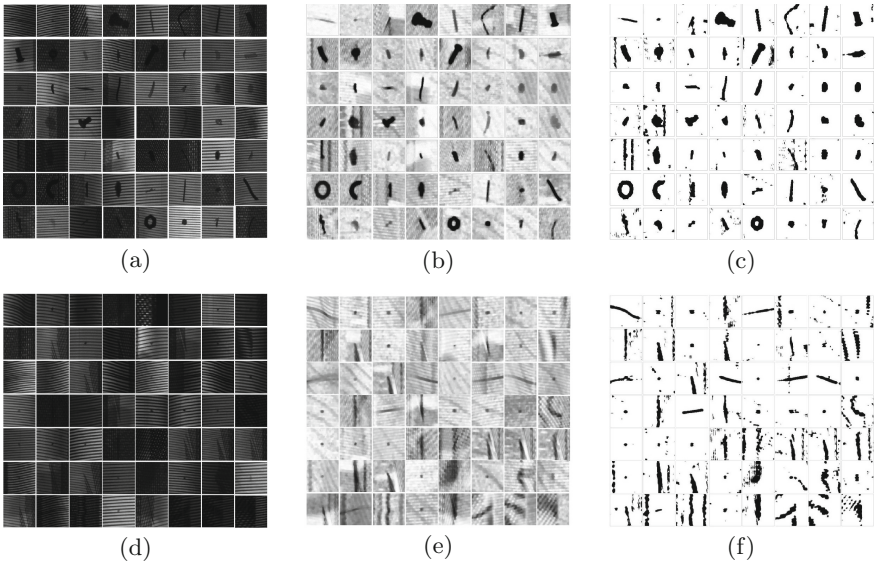

Fig. 3. Positive impurity samples (a–c) and negative impurity samples (d–f). (a, d) in source image, (b, e) in column-equalized image, (c, f) in binary image.

Based on these observations, we propose to extract five kinds of features from three domains as follows. The three domains are: (1) the source tire image, (2) the column-equalized image, where histogram equalization is carried out column-by-column on the source image, and (3) the binary image obtained from Sect. 2.1. Blobs are simultaneously extracted from all the three domains and normalized to the same resolution of 120 × 120, as depicted in Fig. 3. As for the five kinds of features, they are: (1) a 256-d color histogram to represent the blob's statistical information in the HSI space; (2) a 360-d gabor wavelet feature that is invariant to affine transformations and high resistance to noise [11]; (3) a 576-d histogram of oriented gradient (HOG) feature that efficiently captures the local shape statistics [12]; (4) a 52-d LBP feature and (5) a 8-d gray level co-occurrence matrix (GLCM) feature to express the blob texture [13]. By extracting the five kinds of features on the three domains, we obtain 15 groups of feature vectors describing the blobs from different aspects. These feature vectors constitute a complete but redundant representation for the candidate blobs.

2.3 Multiple Kernel Learning Module

The traditional support vector machine (SVM) is a discriminative classifier proposed for binary classification problems. Let $\{(\mathbf{x}_i, y_i)\}_i^N$ denotes a sample of N independent and identically distributed training instances. $\mathbf{x}_i$ is the D-dimensional vector and $y_i \in \{-1, +1\}$ is its class label. Let assume the mapping function $\boldsymbol{\Phi} : \mathbb{R}^D \rightarrow \mathbb{R}^S$. The discriminating hyperplane can be represent as formulation (1). So the classifier can be trained by solving the quadratic optimization problem function (2):

$$\langle \mathbf{w}, \Phi(\mathbf{x}_i) \rangle + b = 0 \tag{1}$$

$$\begin{aligned} \min \quad & \frac{1}{2} \|\mathbf{w}\|_2^2 + C \sum_{i=1}^{N} \xi_i \\ s.t. \quad & y_i \left(\langle \mathbf{w}, \Phi(x_i) \rangle + b \right) \geqslant 1 - \xi_i \\ & \xi_i \geqslant 0, \ \forall i = 1, ..., N \end{aligned} \tag{2}$$

While $\mathbf{w}$ is the vector of weight coefficients, C is given misclassification penalty which maximises the margin while minimising the hinge loss on training set $\{(\mathbf{x}_i, y_i)\}$. ξ is the vector of slack variables, and b is the bias term of the separate hyperplane. However, we always employ the Lagrangian dual function to solve this problem indirectly since it will turn the tough problem to be much easier.

$$\begin{aligned} \max \quad & \sum_{i=1}^{N} \boldsymbol{\alpha}_i - \frac{1}{2} \sum_{i=1}^{N} \sum_{j=1}^{N} \boldsymbol{\alpha}_i \boldsymbol{\alpha}_j y_i y_j \underbrace{\langle \boldsymbol{\Phi}(\mathbf{x_i}), \boldsymbol{\Phi}(\mathbf{x_j}) \rangle}_{k(\mathbf{x}_i, \mathbf{x}_j)} \\ s.t. \quad & \sum_{i=1}^{N} \boldsymbol{\alpha}_i y_i = 0, \quad C \geqslant \boldsymbol{\alpha}_i \geqslant 0 \quad \forall i = 1, ...N \end{aligned} \tag{3}$$

Where $k : \mathbb{R}_D \times \mathbb{R}_D \rightarrow \mathbb{R}$ is called the *kernel function* and $\boldsymbol{\alpha}_i$ and $\boldsymbol{\alpha}_j$ are the vectors of dual variables respectively corresponding to each separation constraint. Then we can get $\mathbf{w} = \sum_{i=1}^{N} \alpha_i y_i \boldsymbol{\Phi}(\boldsymbol{x_i})$ after solving formulation (3) above. So, the new discriminant function can be rewritten as following:

$$f(\mathbf{x}) = \sum_{i=1}^{N} \boldsymbol{\alpha}_i y_i k(\boldsymbol{x}_i, \boldsymbol{x}_j) + b \tag{4}$$

Unlike SVM classification that performs learning based on a single kernel, MKL uses multiple kernels to perform the learning. Mathematically, assume $\mathbf{X}_i = \{\mathbf{x}_i^m\}_{m=1}^P$ the feature matrix of the i^{th} instance with P kinds of feature descriptors. So, we train distance functions $f_1, ..., f_P$ at first, the descriptors and distance functions are then "kernelised" to yield base kernels matrices $\boldsymbol{K}_1, ..., \boldsymbol{K}_P$. Then the optimal kernel combination is approximated by

$\boldsymbol{K}_{opt} = \sum_{m=1}^{P} \eta_m \boldsymbol{K}_m$, where parameters $\boldsymbol{\eta}$ adjust the weights of different features. Similar to SVM, the optimization objective is to achieve the best classification performance. The objective function can be written as:

$$\begin{aligned} J(\boldsymbol{\eta}) = min \quad & \frac{1}{2}\|\boldsymbol{W}_\eta\|_2^2 + C\sum_{i=1}^{N}\boldsymbol{\xi}_i + \sum_{m=1}^{P}\boldsymbol{\delta}_m\boldsymbol{\eta}_m \\ s.t. \quad & y_i\left(\langle \mathbf{w}_\eta, \Phi_e ta(x_i)\rangle + b\right) \geqslant 1 - \xi_i \\ & \boldsymbol{\xi} \geqslant 0, \boldsymbol{\eta} \geqslant 0, \quad \forall i = 1, ..., N \\ & \boldsymbol{W}_\eta \in \boldsymbol{R}^{\boldsymbol{S}_\eta}, \boldsymbol{\xi} \in \boldsymbol{R}_+^N, b \in \boldsymbol{R}, \delta \in \boldsymbol{R}_+^P \end{aligned} \tag{5}$$

To tackle this optimization problem, we adopt the minimax optimization strategy of [14]. In the method, the primal strategy is to minimise $J(\eta)$ through the iteration $\boldsymbol{\eta}^{n+1} = \boldsymbol{\eta}^n - \varepsilon^n \nabla J$ under the constraints $\boldsymbol{\eta} \geqslant 0$. The minimax algorithm consists of two iterative stages. First, let η fixed and therefore $\boldsymbol{K} = \sum_{m=1}^{P} \eta_m \boldsymbol{K}_m$ are also fixed. $\boldsymbol{W}$ is a standard SVM dual with kernel matrix $\boldsymbol{K}$ as $\sum_{m=1}^{P} \boldsymbol{\delta}\boldsymbol{\eta}_m$ is a constant. Second, minimise J by projected gradient descent algorithm and get the optimal weight parameters. The two steps are repeated iteratively until it is convergenced or a fixed number of iterations is reached. With the learned weights and parameters, a new sample $\boldsymbol{X}$ can be classified by the decision function $sign\left(\sum_{i=1}^{N} \boldsymbol{\alpha}_i y_i K_i(\boldsymbol{X}, \boldsymbol{X}_i) + b\right)$.

3 Experiments

To evaluate the effectiveness of the proposed idMKL method, we collect a dataset containing over 5000 tire X-ray images from a large tire factory. In the dataset, there are 550 images containing different impurities, while the rest 4500 ones are images without impurity defect. The width of the images ranges from 2200 to 2700, while their height ranges from 10800 to 12400. All pixels are with 256 gray levels. The images cover dozens of major tire models. We take *Detected Rate* (DR) and *Error Rate* (ER) as the evaluation metrics [3]. Assume P_c and P_m are the number of impurity images that are detected and missed by the algorithm, respectively, while N_a and N_e are the number of normal images that are detected as normal and impurity images respectively, the two metrics are defined as:

$$DR = \frac{P_c}{P_c + P_m}, ER = \frac{N_e}{N_a + N_e} \tag{6}$$

Obviously, higher DR indicates the algorithm is less likely to miss true impurities, while lower ER implies less efforts are required to double check the reported tires. We first evaluate effectiveness of the 15 features individually. By merely using image processing techniques described in Sect. 2.1 to the 4500 impurity-free images, 580 false alarm blobs are collected. We also crop 566 impurity blobs from the 550 impurity images. The two sets of blobs are first randomly split following the fixed ratios of 7:3. They are then mixed accordingly to constitute the training

Table 1. SVM classification result on the collected dataset.

(a) Source image results					
SourIm	GLCM	LBP	HOG	HSI	Gabor
DR	0.834	0.72	0.55	0.705	0.808
ER	0.008	0.012	0.025	0.015	0.012
(b) Column-equalized image results					
ColeIm	GLCM	LBP	HOG	HSI	Gabor
DR	0.852	0.745	0.502	0.725	0.832
ER	0.005	0.016	0.02	0.012	0.01
(c) Binary image results					
BinaIm	GLCM	LBP	HOG	HSI	Gabor
DR	0.738	0.746	0.570	0.550	0.788
ER	0.005	0.015	0.02	0.01	0.018

Table 2. The performance of impurity detection.

Data	IP		bSVM		aSVM		idMKL	
	DR	ER	DR	ER	DR	ER	DR	ER
D550	0.973	0.091	0.955	0.044	0.960	0.040	0.964	0.033
D4500	NA	0.093	NA	0.055	NA	0.055	NA	0.044

and testing sets. Table 1 gives the experimental results. In the table, SourIm, ColeIm and BinaIm denote the source tire image, column-equalized image and the binary image, respectively.

From the table we can see that all the 15 features can distinguish the impurity to some extent, not only correctly classifying non-impurities, but also classifying a few impurities as non-impurities. Since GLCM on ColeIm achieves the highest DR and lowest ER, we fix the setting as the bSVM and will further analyze it in the following experiments.

We then evaluate different methods on the image-level impurity detection. Specifically, four groups of evaluations are carried out. (1) IP: using image processing techniques purely to get the result, i.e., all candidate blobs obtained from Sect. 2.1 are regarded as impurities; (2) bSVM: the setting achieves the best performance when evaluating the 15 features individually; (3) aSVM: all the 15 features are concatenated to form a single feature vector. SVM classification is then applied to get the result; (4) the proposed idMKL method. Impurity detection results of the four methods are given by Table 2. In the table, for the sake of better explaining the methods, we show the results on impurity and non-impurity images separately, i.e., D550 and D4500 are the collection of impurity images and impurity-free images, respectively. Moreover, since DR is meaningless for impurity-free images, we place "NA" in the corresponding position.

As can be seen, compared with the IP baseline, bSVM reduces ER but its DR is also reduced. aSVM get slightly better performance than bSVM. idMKL get better results than aSVM and bSVM on both DR and ER, which clear validate the superior of leveraging MKL. Interestingly, only a marginal improvement is observed when comparing aSVM with bSVM. This can be explained as the concatenated vector, despite more complete, also contains many redundant information that is not helpful to the SVM learning. It is observed that 3.6% of impurities are missed by idMKL, from which 75% are missed by the IP process while the rest 25% are wrongly classified by MKL. This prohibits idMKL to be a fully automatic system currently, as the objective of quality inspection is to discover the impurity such that ideally, DR should approach 100%. On the other hand, since idMKL already achieves promising results. It has been adopted as a complementary way to the manual inspection by tire factories, i.e., tires images passed the human inspection are double checked by our idMKL method, workers are asked to check again when there are impurities reported. Encouraging feedbacks are reported: Human inspection only discover 0.9% defect tires, while the ratio reported by idMKL and further confirmed by workers are 1.5%. That is to say. idMKL is a complementary or even more reliable method than humans in impurity defect detection.

In Fig. 4, we also sort the weights of different features learned by idMKL. Similar to previous observations, GLCM and Gabor on ColeIm are ranked at the top. On the contrary, the weights for LBP, HIS, HOG on BinaIm are negligible. Their classification ability is well covered and replaced by other features. This also explains the redundant nature of the extracted features.

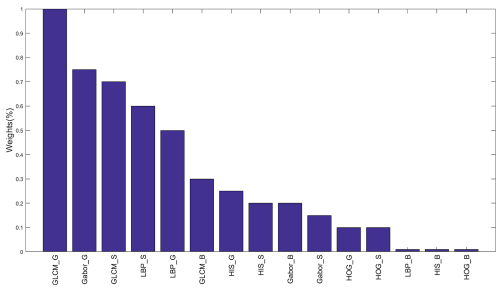

Fig. 4. The kernel weights rank of different features.

4 Conclusion

Automatic tire quality inspection is strongly demanded by tire industry to replace the manual inspection. In this paper, we propose an efficient tire impurity detection method named idMKL to approach this goal. idMKL is featured by leveraging MKL to adaptively combine the discriminative features from a complete but noisy feature pool. Experimental results on thousands of tire images basically validate that idMKL can effectively classify impurity and non impurity

blobs. idMKL is also shown to be more useful than human in inspecting tire impurities. However, idMKL is limited by the fact that its DR is still not perfect. Thus, future work includes studies on further enhancing DR. Besides, we are also interested in developing methods towards automatically detect more kinds of defects such as bubbles, and investigating schemes that are more suitable for industrial environments [15,16] in the near future.

References

1. Guo, Q., Wei, Z.: Tire defect detection using image component decomposition. Res. J. Appl. Sci. Eng. Technol. **4**(1), 41–44 (2012)
2. Zhang, Y., Li, T., Li, Q.: Defect detection for tire laser shearography image using curvelet transform based edge detector. Opt. Laser Technol. **47**(4), 64–71 (2013)
3. Zhang, Y.: Research on nondestructive tire defect detection using computer vision methods. Ph.D. thesis, Qingdao University of Science and Technology (2014). (in Chinese)
4. Zhang, Y., Dimitr, L., Li, Q.L.: Automatic detection of defects in tire radiographic image. IEEE Trans. Autom. Sci. Eng. 1–9 (2017, accepted)
5. Xiang, Y., Zhang, C., Guo, Q.: A dictionary-based method for tire defect detection. In: IEEE International Conference on Information and Automation, pp. 519–523 (2014)
6. Tajeripour, F., Kabir, E., Sheikhi, A.: Fabric defect detection using modified local binary patterns. EURASIP J. Adv. Sign. Process. **2008**(1), 1–12 (2007)
7. Kumar, A.: Computer-vision-based fabric defect detection: a survey. IEEE Trans. Indus. Electron. **55**(1), 348–363 (2008)
8. Cui, X., Liu, Y., Wang, C., Li, H.: A novel method for feature extraction and automatic recognition of tire defects. In: ICIMM International Conference on Intelligent Manufacturing and Materials, pp. 1–9 (2016)
9. Qiu, S., Lane, T.: A framework for multiple kernel support vector regression and its applications to sIRNA efficacy prediction. IEEE/ACM Trans. Comput. Biol. Bioinform. **6**(2), 190–199 (2009)
10. Kumar, A., Sminchisescu, C.: Support kernel machines for object recognition. In: IEEE International Conference on Computer Vision, pp. 1–8 (2007)
11. Ke, Y., Youbin, C., David, Z.: Gabor surface feature for face recognition. In: Pattern Recognition, pp. 288–292 (2011)
12. Dalal, N., Triggs, B.: Histograms of oriented gradients for human detection. In: IEEE Computer Society Conference on Computer Vision and Pattern Recognition, pp. 886–893 (2005)
13. Crosier, M., Griffin, L.D.: Using basic image features for texture classification. Int. J. Comput. Vis. **88**(3), 447–460 (2010)
14. Varma, M., Ray, D.: Learning the discriminative power-invariance trade-off. In: IEEE International Conference on Computer Vision, pp. 1–8 (2007)
15. Gao, X., Gu, Z., et al.: ContainerLeaks: emerging security threats of information leakages in container clouds. In: IEEE International Conference on Dependable Systems and Networks, pp. 1–12 (2017)
16. Gao, X., Liu D., et al.: E-Android: a new energy profiling tool for smartphones. In: 37th IEEE International Conference on Distributed Computing Systems, pp. 492–502 (2017)